Original Article

Three-dimensional pseudocontinuous arterial spin labeling with dual postlabeling delay for reflecting cerebral blood flow regulation in patients with hydrocephalus: a retrospective cross-sectional study

Yawen Xiao[1#^], Shiqi Chen[1,2#^], Zhaotao Zhang[1], Jianglong Huang[1], Yifei Gui[1], Dan Luo[1], Xinru Deng[1], Jiankun Dai[3], Xinlan Xiao[1^]

[1]Department of Radiology, The Second Affiliated Hospital of Nanchang University, Nanchang, China; [2]Department of Nuclear Medicine, First Affiliated Hospital of Nanchang University, Nanchang, China; [3]GE Healthcare, MR Research China, Beijing, China

Contributions: (I) Conception and design: X Xiao, Y Xiao; (II) Administrative support: X Xiao, Z Zhang, J Dai; (III) Provision of study materials or patients: J Huang; (IV) Collection and assembly of data: S Chen, Y Gui, D Luo, X Deng; (V) Data analysis and interpretation: Y Xiao, S Chen; (VI) Manuscript writing: All authors; (VII) Final approval of manuscript: All authors.

[#]These authors contributed equally to this work.

Correspondence to: Xinlan Xiao, MS. Department of Radiology, The Second Affiliated Hospital of Nanchang University, No. 1 Minde Road, Donghu District, Nanchang 330008, China. Email: jx_xiaoxinlan@sina.com.

Background: Three-dimensional pseudo-continuous arterial spin-labeling (3D pCASL) with dual postlabeling delay (PLD) captures both early and delayed cerebral blood flow (CBF), yet its potential in reflecting blood flow regulation in hydrocephalus patients remains uncertain. This study investigated the hemodynamic characteristics in patients with hydrocephalus and whether the difference in cerebral blood flow using short and long PLDs (ΔCBF = CBFPLD =2.5 s – CBFPLD =1.5 s) could reflect cerebral regulation and further aimed to demonstrate the associations between regional ΔCBF and the degree of ventricular dilatation.

Methods: This retrospective study included consecutive patients with hydrocephalus and control participants attending The Second Affiliated Hospital of Nanchang University from December 2017 to December 2022. The CBF in 18 brain regions was manually delineated by two radiologists. Regional CBF and ΔCBF were compared via covariance analyses. The associations between ΔCBF and the degree of ventricular dilatation were investigated using linear regression analyses and interaction analysis.

Results: In total, 58 patients with communicating hydrocephalus, 57 patients with obstructive hydrocephalus, and 52 controls were analyzed. CBF of the hydrocephalus groups was lower than that of the control group at the shorter PLD. CBF was higher at a longer PLD, with no difference between the hydrocephalus groups and the control group in some regions. The hydrocephalus groups showed a higher ΔCBF compared to the control group. Furthermore, in the left medial watershed (10.6±5.66 *vs.* 7.01±5.88 mL/100 g/min; P=0.038), communicating hydrocephalus exhibited greater ΔCBF than did obstructive hydrocephalus. ΔCBF of the right posterior external watershed [adjusted β: 0.276; 95% confidence interval (CI): 0.047–0.505; P=0.019] and right parietal cortex (adjusted β: 0.277; 95% CI: 0.056–0.498; P=0.015) in the obstructive hydrocephalus group and ΔCBF of the left internal watershed (adjusted β: 0.274; 95% CI: 0.013–0.536; P=0.040) in the communicating hydrocephalus group were associated with the

^ ORCID: Xinlan Xiao, 0000-0001-9701-5062; Yawen Xiao, 0000-0003-4291-6589; Shiqi Chen, 0000-0003-0821-986X.

degree of ventricular dilatation, respectively.

Conclusions: Patients with hydrocephalus showed cerebral regulation in maintaining adequate CBF, resulting in longer arterial transit times. The ability to regulate CBF in brain regions represented by the watershed was associated with the degree of ventricular dilation.

Keywords: Hydrocephalus; three-dimensional pseudo-continuous arterial spin-labeling (3D pCASL); cerebral blood flow (CBF); cerebral blood flow regulation (CBF regulation); hemodynamics

Submitted Jan 25, 2024. Accepted for publication Jun 18, 2024. Published online Jul 30, 2024.
doi: 10.21037/qims-24-151
View this article at: https://dx.doi.org/10.21037/qims-24-151

Introduction

Hydrocephalus is a pathological state that has various causes and is mainly classified into obstructive hydrocephalus and communicating hydrocephalus types (1). Overproduction of cerebrospinal fluid (CSF) or disorders in its circulation and absorption can lead to abnormal ventricular expansion, which is usually accompanied by an increase in intracranial pressure (ICP) (2). Elevated ICP and ventriculomegaly can lead to secondary neurovascular injury, exacerbating tissue damage and hindering brain development. Additionally, ventriculomegaly may lead to the compression and extension of periventricular tissues (including axons, myelin, and vessels), leading to ischemia, hypoxia, inflammation, and subsequent metabolic disorders and alterations in the permeability of the blood-brain barrier (3). Cerebral palsy, claudication, urinary incontinence, and vision loss will occur if hydrocephalus is not treated promptly. In the acute stage, increased ICP may lead to brain herniation, which is a life-threatening condition (4).

Research has identified that ventriculomegaly may directly reduce cerebral blood flow (CBF) through mechanical traction and vascular caliber reduction (5,6). Previous studies have used single photon emission computed tomography (SPECT), positron emission tomography (PET), computed tomography perfusion (CTP), and dynamic susceptibility contrast magnetic resonance imaging (MR DSC) to confirm that the CBF of hydrocephalus patients is lower than normal. However, these techniques all rely on the invasive administration of radioactive tracers or contrast agents (7-9). Moreover, these studies have not determined whether the brain of those with hydrocephaly, who may experience hypoperfusion, ischemia, and hypoxia, employs mechanisms to regulate and maintain adequate CBF. Some research has been conducted on the regulation of CBF in hydrocephalus using transcranial Doppler (TCD) (10). However, although TCD can measured the hemodynamics of intracranial primary vessels, it cannot quantify blood flow regionally. Additionally, TCD needs to be combined with cerebral perfusion pressure and CSF outflow resistance to reflect the dynamics of cerebrovascular regulation in patients with hydrocephalus (10).

Three-dimensional pseudo-continuous arterial spin-labeling (3D pCASL) is a noninvasive magnetic resonance imaging (MRI) technique for detecting CBF (11,12). The CBF of healthy individuals across different ages and patients with various diseases can be measured more accurately and reproducibly by setting the suitable postlabeling delay (PLD) (13). However, although the single PLD method provides information on CBF, it does not reflect the characteristics of early and late CBF at different PLDs. The acquisition of multiple PLDs allows for the differentiation of various components of the CBF signal, including arterial transit time (ATT) effects. Observers can better capture the dynamics of blood flow and improve the accuracy of CBF quantification. However, obtaining multiple PLDs is more complicated due to long the scanning time and complex postprocessing (13). At present, the combination of long- and short-PLD dual-phase arterial spin-labeling (ASL) has been used in the study of ischemic, vascular, and neurodegenerative disease (14-16). When the blood flows slowly, the labeled blood cannot fully flow through in the short PLD, while prolonging the PLD allows for the slowly flowing blood to reach its destination (17). By analyzing the difference in measured CBF at two different PLDs [delta cerebral blood flow (ΔCBF)], we can discern the difference between early and late perfusion.

We hypothesized that ventriculomegaly in patients with hydrocephalus may compress the brain parenchyma, potentially leading to vascular regulation changes and alterations in cerebral hemodynamics. Therefore, we

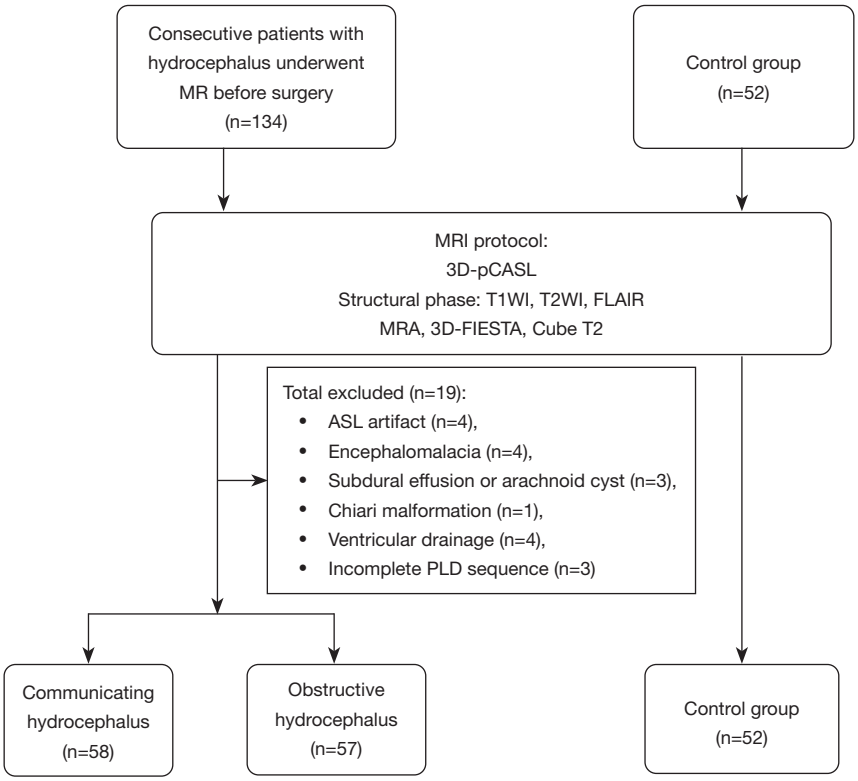

Figure 1 Participant inclusion and exclusion flowchart. MR, magnetic resonance; MRI, magnetic resonance imaging; 3D pCASL, three-dimensional pseudo-continuous arterial spin-labeling; T1WI, T1-weighted imaging; T2WI, T2-weighted imaging; FLAIR, fluid-attenuated inversion recovery; MRA, MR angiography; 3D FIESTA, three-dimensional fast imaging employing steady-state acquisition; ASL, arterial spin-labeling; PLD, postlabeling delay.

attempted to use 3D pCASL with dual PLDs to investigate the hemodynamic characteristics in patients with hydrocephalus to determine whether ΔCBF can reflect cerebral regulation and to clarify the association between ΔCBF in different regions of brain and the degree of ventricle dilation. We present this article in accordance with the STROBE reporting checklist (available at https://qims.amegroups.com/article/view/10.21037/qims-24-151/rc).

Methods

This study was conducted in accordance with the Declaration of Helsinki (as revised in 2013), approved by the Ethics Committee of The Second Affiliated Hospital of Nanchang University, and registered in the Clinical Trials Register number (http://www.chictr.org.cn; registration No. ChiCTR2300070646). All participants were exempted from informed consent due to the study's retrospective nature.

Participants

Data from consecutive patients with hydrocephalus who underwent MR before hydrocephalus surgery at The Second Affiliated Hospital of Nanchang University between December 2017 and December 2022 were retrospectively collected. The exclusion criteria were as follows: (I) presence of ASL artifacts due to head movement or dentures, (II) encephalomalacia (more than 1 cm in diameter), (III) intracranial arachnoid cysts, (IV) hydrocephalus due to cerebellar tonsillar herniation, and (V) cervical or cranial vascular stenosis (more than 25% on visual inspection). Meanwhile, volunteers without hydrocephalus or neurological symptoms were included as the control group (*Figure 1*).

Imaging review

Based on the high-resolution sagittal three-dimensional fast imaging employing steady-state acquisition (3D FIESTA) and CUBE T2 sequence, it was determined whether there was an obstruction in the third ventricle, aqueduct, or fourth ventricle outflow pathway in patients obstructive hydrocephalus. Those without obvious obstructions were classified as communicating hydrocephalus if the Evans index was greater than 0.3 on the MR plain scans (18). These assessments were completed by a neuroradiologist (J.H., with 9 years' experience). Indeterminate cases were classified after discussion with an expert neuroradiologist (X.X., with 34 years' experience). The diffusion-weighted imaging (DWI) sequence was reviewed to exclude recent cerebral infarction (Y.X., with 9 years' experience). MR angiography (MRA) was reviewed to identify cerebral vascular conditions (S.C., with 3 years' experience).

MRI protocol

Images were acquired on a 3.0T-MR scanner (Discovery 750w, GE HealthCare, Chicago, IL, USA) with a 19-channel head and neck unit coil. All participants were placed in a supine position and fixed with sponge-rubber pads to limit head motion. The MRI protocol included 3D FIESTA, CUBE T2, DWI, MRA, T1-weighted imaging (T1WI), T2-weighted imaging (T2WI), fluid-attenuated inversion recovery (FLAIR), and 3D pCASL with dual PLDs (1.5 and 2.5 s). The specific scanning parameters are shown in Table S1.

Imaging processing

The 3D pCASL was processed with a vendor-provided workstation (Advantage Workstation 4.7; GE HealthCare).

Quantification was performed using the two-compartment model (19). The following flow calculation formula was applied (20,21):

$$f = \frac{\lambda}{2\alpha T_{1b}\left(1-e^{\frac{\tau}{T_{1b}}}\right)} \frac{\left(S_{ctrl}-S_{1bl}\right)\left(1-e^{-\frac{t_{sat}}{T_{1g}}}\right)}{S_{ref}} e^{\frac{\omega}{T_{1b}}} \quad [1]$$

where f is the flow, multiplied by a scaling factor (6,000,000) and converted to physiological units of mL/100 cc gray matter/min; S is the acquired signal on the control (ctrl) and labeled (1bl) signal or the reference image; T1b and T1g are the T1 values of blood and gray matter, respectively; α is the labeling efficiency; λ is the cortex-blood partition coefficient; and τ and ω represent the labeling duration (1,450 msec) and post-labeling delay time (1,500 or 2,500 msec), respectively. We used the T1 of blood (1,600 ms at 3T) (22), labeling efficiency (α=0.85), and the blood-brain partition coefficient (λ=0.9 mL/g) (23) for the pCASL.

The source images of 3D pCASL were coregistered to anatomical T2WI or 3D T1 brain volume (BRAVO) images using rigid registration. Subsequently, the CBF maps were coregistered to the anatomical images via direct application of the coregistration information. The coregistered CBF maps were further overlayed on the anatomical images, and manual adjustment was performed as necessary. The region of interest (ROI) was then manually delineated on the anatomical images to obtain the CBF values. All brain regions (*Figure 2*) of the above CBF maps were outlined on two consecutive slices independently by two neuroradiologists (Y.X. and S.C., with 9 and 3 years' experience, respectively) who were blinded to patients' grouping information (*Figure 3*). In this study, ROIs were selected to include the bilateral anterior external watershed, posterior external watershed, internal watershed, frontal cortex, parietal cortex, temporal cortex, occipital cortex, thalamus, and cerebellar hemispheres. Referring to Hou *et al.*'s research (24), we delineated the frontal cortex, parietal cortex, temporal cortex, and occipital cortex. According to Li *et al.*'s study (25), we placed ROIs on the anterior external watershed, posterior external watershed, and internal watershed. The anterior and posterior external watersheds included ovoid ROIs on one to two layers above the basal ganglia (26). The white matter at the centrum semiovale and alongside the lateral ventricle were outlined as the ROI of the internal watershed. *Figure 4* illustrates examples of the CBF estimate in three groups of patients at PLDs of 1.5 and 2.5 s. ΔCBF was considered to be the difference in measured CBF at two different PLDs and was calculated as follows: $\Delta CBF = CBF_{PLD\ =2.5\ s} - CBF_{PLD\ =1.5\ s.}$ The Evans index (Figure S1), representing the degree of ventricular dilation (27), was obtained by averaging the measurements of two neuroradiologists (Y.G. and D.L., with 3 and 2 years' experience, respectively).

Statistical analysis

Statistical analysis was performed with SPSS version 26.0 (IBM Corp., Armonk, NY, USA) and R version 4.1.3 (The R Foundation for Statistical Computing; https://www.

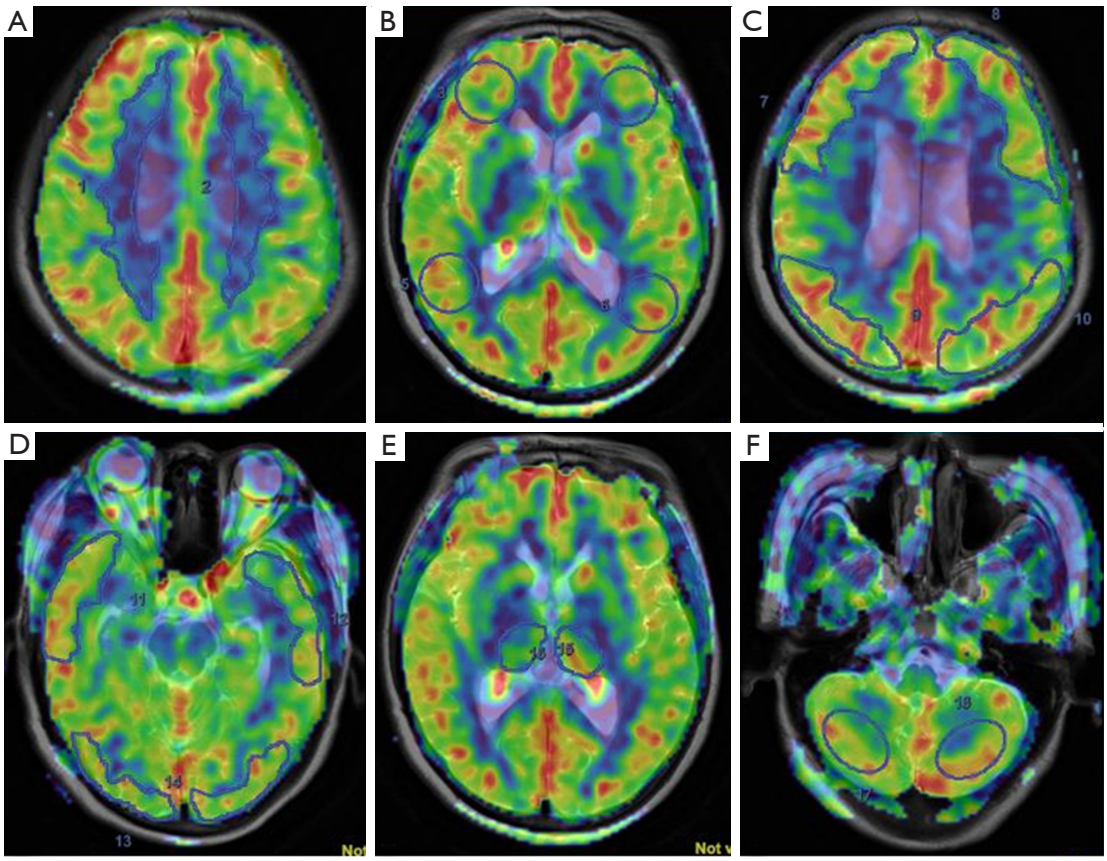

Figure 2 Selection and delineation of ROIs. (A) ROI 1 and ROI 2 respectively represent the right and left internal watershed. (B) ROI 3 and ROI 4 respectively represent the right and left anterior external watershed, and ROI 5 and ROI 6 respectively represent the right and left posterior external watershed. (C) ROI 7 and ROI 8 respectively represent the right and left frontal cortex, and ROI 9 and ROI 10 respectively represent the right and left parietal cortex. (D) ROI 11 and ROI 12 respectively represent the right and left temporal cortex, and ROI 13 and ROI 14 respectively represent the right and left occipital cortex. (E) ROI 16 and ROI 15 respectively represent the right and left thalamus. (F) ROI 17 and ROI 18 respectively represent the right and left cerebellum. ROI, region of interest.

r-project.org). For continuous measures, the Shapiro-Wilk test was used to perform a normality test, and differences between groups were assessed via one-way analysis or the Kruskal-Wallis test. A χ^2 test was used to compare the frequency distributions of sex, clinical symptoms, and comorbidities. The intraobserver reproducibility was calculated using the intraclass correlation coefficient (ICC) and coefficient of variation (CV). Differences in CBF and ΔCBF between the groups were compared using covariance analysis, with post hoc Bonferroni tests used to correct for multiple comparison and with age being controlled for. Linear regression analyses were performed in the communicating and obstructive hydrocephalus groups, respectively, to assess the relationships between ΔCBF and ventricular dilatation after adjustments were for age, sex, and duration. To further eliminate the effect of age on the CBF of hydrocephalus, the interaction between age and the different hydrocephalus groups was analyzed using the control group as a reference. The "Fdrtool" package in R was applied to adjust for multiple testing, and the P value was corrected with the false discovery rate (FDR). All tests were two-tailed, and $P<0.05$ was considered to indicate a significant difference. The detailed sample size calculations are provided in Appendix 1.

Results

Participant characteristics

After exclusions (*Figure 1*), 58 patients with communicating

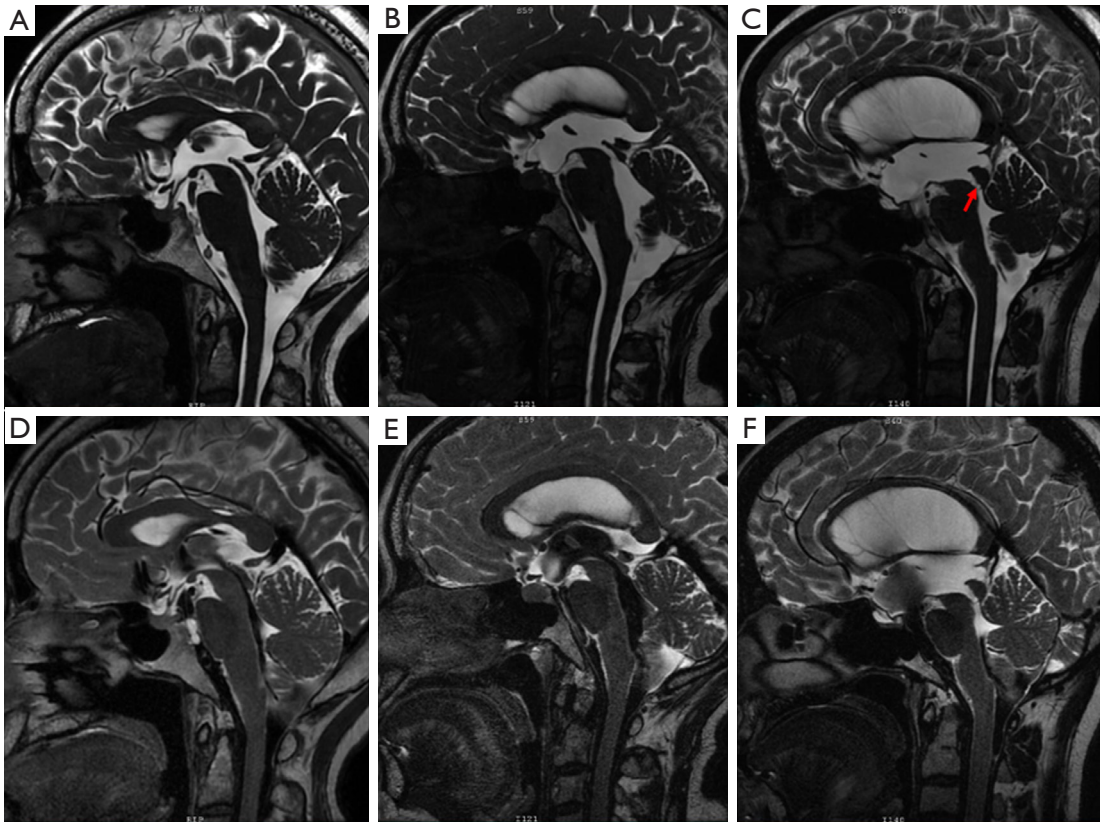

Figure 3 Representative images. (A-C) 3D FIESTA images and (D-F) CUBE images. (A,D) A 55-year-old female healthy volunteer. The ventricular system was not dilated, and the aqueduct and outflow tract of the fourth ventricle were patent (CUBE showed a flow-void signal). (B,E) A 42-year-old female with communicating hydrocephalus. The ventricles were dilated, and the aqueduct and fourth ventricle outflow tracts were patent (CUBE showed a flow-through signal). (C,F) A 33-year-old female with obstructive hydrocephalus. The lateral ventricles were significantly dilated, three transverse membranes (red arrow) could be seen at the aqueduct, the aqueduct was obstructed (loss of flow-void signal on CUBE), and the fourth ventricular outflow tract was patent (flow-void signal on CUBE). 3D FIESTA, three-dimensional fast imaging employing steady-state acquisition.

hydrocephalus [24 women (41%), including 1 patient with secondary communicating hydrocephalus after aneurismal subarachnoid hemorrhage, 2 patients with secondary communicating hydrocephalus after traumatic intracerebral hemorrhage, 55 patients with primary communicating hydrocephalus], 57 patients with obstructive hydrocephalus [28 women (49%), including 39 patients with aqueductal stenosis, 12 patients with fourth ventricle outlet stenosis, 6 patients with interventricular foramen occlusion of lateral ventricle], and 52 controls [26 women (50%)] were included in the final analyses.

The baseline characteristics of participants are summarized in *Table 1*. There was no significant difference in sex between the three groups (P=0.6). Patients with communicating hydrocephalus were older than patients with obstructive hydrocephalus and controls (communicating hydrocephalus: median age 61.5 years, IQR 48–68 years; obstructive hydrocephalus: median age 46 years, IQR 29–57 years; control: median age 49 years, IQR 34–57 years; P<0.001). There were no differences in the duration of disease (since symptom onset), clinical symptoms, comorbidities, or Evans index between the two hydrocephalus groups (P>0.05). In the ICP data obtained from 48 patients with communicating hydrocephalus and 26 patients with obstructive hydrocephalus, it was observed that the ICP in the obstructive hydrocephalus group (median ICP 120 mmH_2O, IQR 85–177.5 mmH_2O) was significantly higher than that in the communicating hydrocephalus group (median ICP 160 mmH_2O, IQR 127.5–222.5 mmH_2O) (P=0.004).

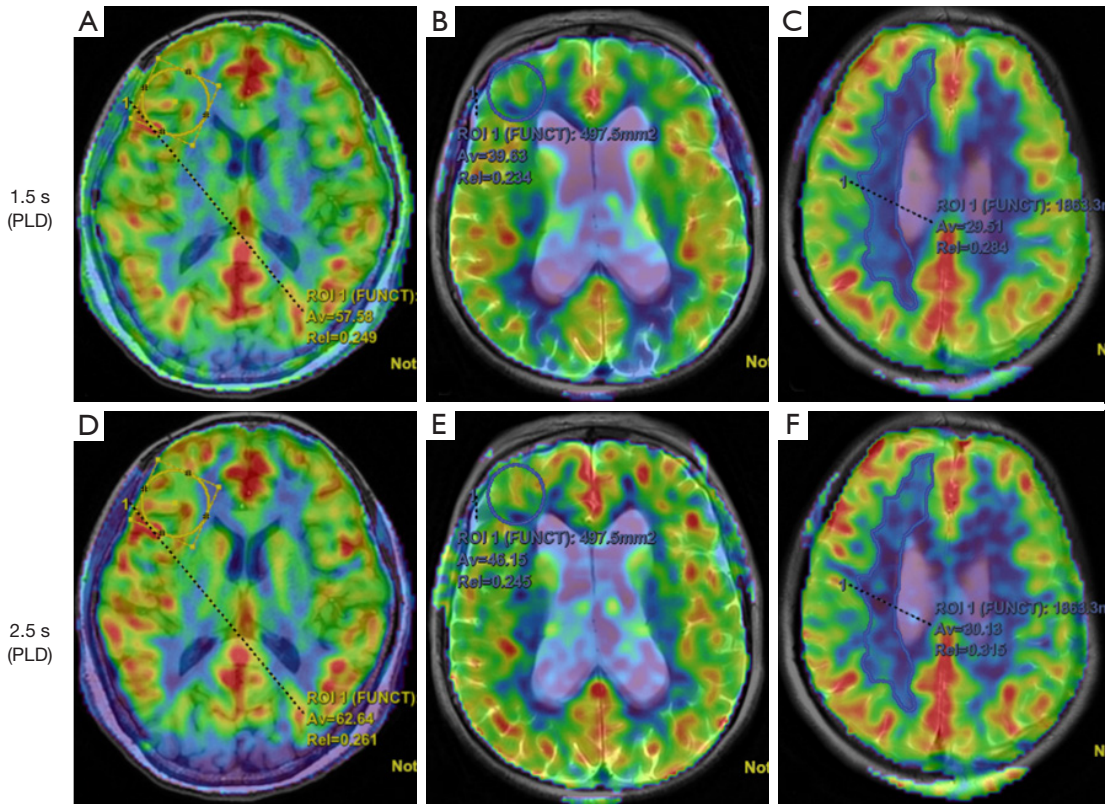

Figure 4 Schematic diagram of the CBF estimate when PLD was 1.5 and 2.5 s. (A,D) A 55-year-old female healthy volunteer. The ROI was placed on the right anterior external watershed. (B,E) A 64-year-old female with obstructive hydrocephalus. The ROI was placed on the right anterior external watershed. (C,F) A 42-year-old female with communicating hydrocephalus. The ROI was placed on the right internal watershed. PLD, postlabeling delay; ROI, region of interest; Av, average; Rel, relative; CBF, cerebral blood flow.

Comparison of CBF and ΔCBF between the groups

The mean ICC of interobserver agreement was 0.91 (95% CI: 0.88–0.94; P<0.001) (Figure S2), and CV was 1.6%, indicating a high degree of agreement between the two neuroradiologists in their manual delineation of the ROIs for CBF value measurement. Covariance analysis with post hoc Bonferroni correction indicated that at a PLD of 1.5 s, CBF in all ROIs decreased successively from the control group to the obstructive hydrocephalus group and the communicating hydrocephalus group. In the communicating hydrocephalus group, the CBF in all brain regions, except the bilateral thalamus, was significantly reduced compared to the control group. In the obstructive hydrocephalus group, the CBF in all brain regions, except the right anterior watershed, left occipital lobe, bilateral cerebellum, and bilateral thalamus, was lower compared to that in the control group. At a PLD of 2.5 s, the CBF was differently elevated in the two hydrocephalus groups compared with that in the control group (*Figure 5*). The increase in CBF in patients with communicating hydrocephalus was more pronounced than that of those with obstructive hydrocephalus. In the communicating hydrocephalus group, CBF in all brain regions, except for the left cerebellum and bilateral thalami, was significantly lower than that in the control group (P<0.05). None of the brain regions, except for the right internal watershed and the left frontal cortex, showed a significant difference in CBF between the obstructive hydrocephalus group and the control group (P>0.05) (*Figure 5*, Tables S2,S3).

The ΔCBF in all ROIs increased successively from the control group to the obstructive hydrocephalus group and communicating hydrocephalus group. Only ΔCBF of left internal watershed in the communicating hydrocephalus group (10.6±5.66 mL/100 g/min) was significantly higher than that in the obstructive hydrocephalus group

Table 1 Patient characteristics in hydrocephalus subtype and control groups

Characteristic	Communicating hydrocephalus[A] (N=58)	Obstructive hydrocephalus[B] (N=57)	Control[C] (N=52)	P value			
				All	A *vs*. B	A *vs*. C	B *vs*. C
Age (y), median (IQR)	61.5 (48–68)	46 (29–57)	49 (34–57)	<0.001***	<0.001***	<0.001***	>0.99
No. of women, n (%)	24 (41.4)	28 (49.1)	26 (50.0)	0.6	NA	NA	NA
Duration (m), median (IQR)	5.5 (1–24)	2 (0.5–12)	NA	NA	0.482	NA	NA
Headache , n (%)	20 (34.5)	16 (28.1)	NA	NA	0.458	NA	NA
Dizziness , n (%)	26 (44.8)	16 (28.1)	NA	NA	0.062	NA	NA
Vomit , n (%)	6 (10.3)	2 (3.5)	NA	NA	0.272	NA	NA
Urinary incontinence , n (%)	6 (10.3)	3 (5.3)	NA	NA	0.490	NA	NA
Gait disturbance , n (%)	15 (25.9)	11 (19.3)	NA	NA	0.400	NA	NA
Weakness of lower limbs , n (%)	5 (8.6)	9 (15.8)	NA	NA	0.240	NA	NA
Hypomnesis , n (%)	9 (15.5)	17 (29.8)	NA	NA	0.067	NA	NA
Hypertension , n (%)	6 (10.3)	4 (7)	NA	NA	0.743	NA	NA
Diabetes , n (%)	2 (3.4)	3 (5.3)	NA	NA	0.679	NA	NA
ICP (mmH_2O)[a], median (IQR)	120 (85–177.5)	160 (127.5–222.5)	NA	NA	0.004	NA	NA
Evans index, mean (SD)	0.355 (0.064)	0.367 (0.094)	0.246 (0.028)	<0.001***	0.850	<0.001***	<0.001***

Duration refers to the persistence of hydrocephalus. [a], data are from 48 patients with communicating hydrocephalus and 26 patients with obstructive hydrocephalus. ***, P<0.001. y, years; IQR, interquartile range; m, months; NA, not applicable; ICP, intracranial pressure; SD, standard deviation.

(7.01±5.88 mL/100 g/min) (P=0.038); the ΔCBF of the other brain regions showed no significant difference between the two hydrocephalus groups (P>0.05) (*Figure 6*, Table S4).

Subgroup analysis: association between ΔCBF and ventricular dilatation

After adjustments were made for age, sex, and duration, the linear regression analysis of the communicating hydrocephalus group indicated that ΔCBF in the right posterior external watershed (adjusted β: 0.260; 95% CI: 0.021–0.499; P=0.034) and left medial watershed (adjusted β: 0.274; 95% CI: 0.013–0.536; P=0.040) was associated with the degree of ventricular dilatation; meanwhile, in the obstructive hydrocephalus group, that ΔCBF in the right posterior external watershed (adjusted β: 0.276; 95% CI: 0.047–0.505; P=0.019) and the right parietal cortex (adjusted β: 0.277; 95% CI: 0.056–0.498; P=0.015) was associated with the degree of ventricular dilatation (*Table 2*).

Through further interaction analysis, an interaction between age and the different hydrocephalus groups was observed with reference to the control group. Specifically, in the aforementioned brain regions, ΔCBF in the left medial watershed was found not to interact with age in the communicating hydrocephalus group (P>0.05). Similarly, ΔCBF in the right posterior external watershed and right parietal cortex did not interact with age in the obstructive hydrocephalus group (P>0.05) (*Table 3*). Thus, ΔCBF in these brain regions may be independently associated with ventricular dilatation in hydrocephalus and not be age-dependent.

Discussion

Our study demonstrated that the observed CBF of the hydrocephalus groups was lower than that of the healthy control group at the shorter PLD. The CBF of the hydrocephalus groups increased with extended PLD but showed no significant difference from that of controls in some regions. The hydrocephalus groups showed a higher ΔCBF compared to the control group. Compared to the obstructive hydrocephalus group, the communicating hydrocephalus group exhibited a notable increase in ΔCBF

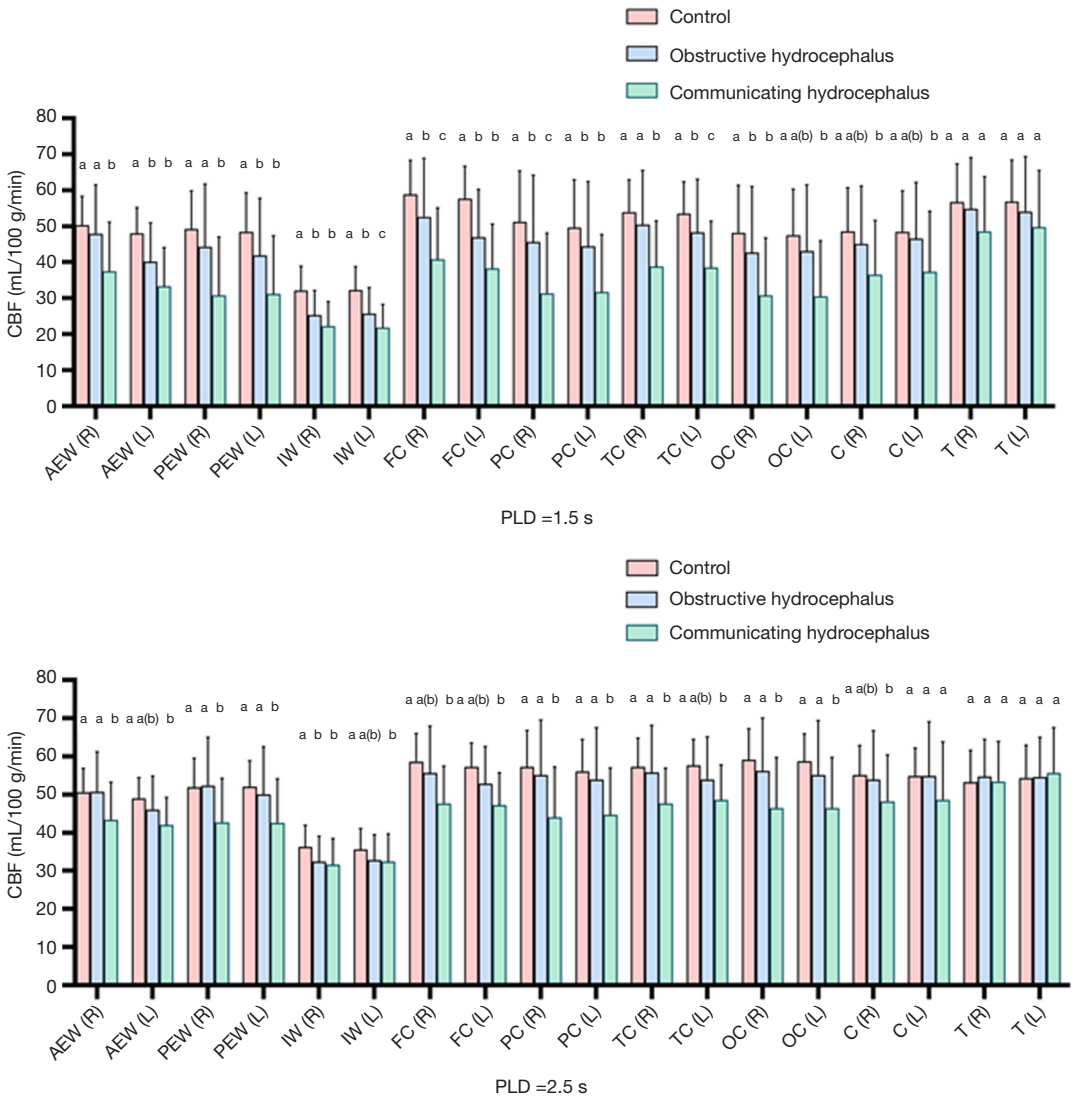

Figure 5 Bar chart with the SD of the CBF for the regional ROIs in the control, obstructive, and communicating hydrocephalus groups. The top panel is the PLD of 1.5 s, and the bottom panel is the PLD of 2.5 s. Letter substitution method was used for marking intergroup differences based on significance, where the same letter indicates no significant difference and different letters indicate significant differences. In certain brain regions, obstructive hydrocephalus is denoted by "a(b)", which indicates that there is no statistical difference in the CBF values between the obstructive hydrocephalus group and both the control group and the communicating hydrocephalus group. However, there was no statistical difference in CBF values between the control group and the communicating hydrocephalus group. CBF, cerebral blood flow; AEW, anterior external watershed; R, right; L, left; PEW, posterior external watershed; IW, internal watershed; FC, frontal cortex; PC, parietal cortex; TC, temporal cortex; OC, occipital cortex; C, cerebellum; T, thalamus; PLD, postlabeling delay; SD, standard deviation; ROI, region of interest.

in the left internal watershed and left temporal cortex. The ΔCBF of the right posterior external watershed right parietal cortex in the obstructive hydrocephalus group, and left internal watershed in the communicating hydrocephalus group was associated with ventricular dilatation.

Consistent with previous studies, our study identified that patients with hydrocephalus had lower CBF than did healthy controls (6,8,28-30). The mechanism of

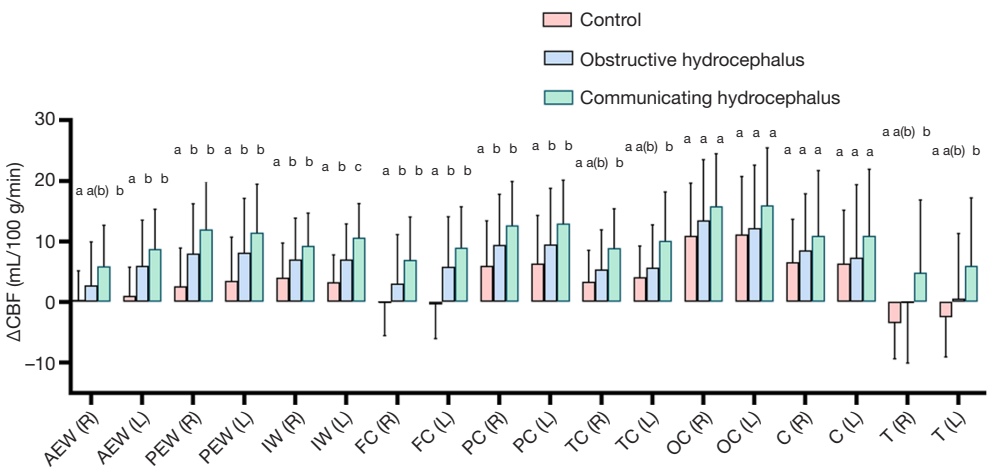

Figure 6 Bar chart with the SD for the ΔCBF in the regional ROIs of the control, obstructive, and communicating hydrocephalus groups. The letter substitution method was used for marking intergroup differences based on significance, where the same letter indicates no significant difference and different letters indicate significant differences. In certain brain regions, obstructive hydrocephalus is denoted by "a(b)", which indicates that there is no statistical difference in the ΔCBF values between the obstructive hydrocephalus group and both the control group and the communicating hydrocephalus group. However, there was no statistical difference in ΔCBF values between the control group and the communicating hydrocephalus group. ΔCBF, delta cerebral blood flow; AEW, anterior external watershed; R, right; L, left; PEW, posterior external watershed; IW, internal watershed; FC, frontal cortex; PC, parietal cortex; TC, temporal cortex; OC, occipital cortex; C, cerebellum; T, thalamus; SD, standard deviation; ROI, region of interest.

CBF reduction in the hydrocephalus region may be multifactorial. The increased ICP due to hydrocephalus leads to reduced perfusion pressure, resulting in phenomena such as lower total CBF in the hydrocephalus group. Additionally, the volume of brain regions may be affected; the expansion of the ventricles in patients with hydrocephalus may cause compression of brain parenchyma, which is another significant factor. Some researchers have pointed out that in hydrocephalus, the migration of CSF results in increased interstitial edema and reduced perfusion (31). Furthermore, the decrease in CBF within the white matter of the brain can lead to a reduction in global CBF (6,31). We further found that patients with communicating hydrocephalus had lower CBF than did patients with obstructive hydrocephalus regardless of the length of PLD. We hypothesize that the lesser reduction in CBF in obstructive hydrocephalus is due to its pathophysiology. As indicated by Greitz *et al.*, ventricle expansion compresses cortical veins, especially near venous sinus outlets, causing venous congestion and increased ICP. Hence, it is also referred to as *venous congestion hydrocephalus* (32). The venous outflow block leads to upstream vasodilation, reducing vascular resistance and resulting in only a minor decrease in CBF during the acute stage (33). Moreover, it is has been reported that obstructive hydrocephalus leads to a higher ICP than does communicating hydrocephalus (34), which is consistent with the findings of our study. During intracranial hypertension, the brain protects itself from hypoperfusion by reducing arterial wall tension (low-to-moderate increase in ICP) or directly increasing perfusion through the Cushing vascular pressure response (steep increase in ICP) (35). When the ICP increases to a certain extent, the brain's protective mechanism leads to an increase in CBF to maintain the oxygen and nutrient supply to the brain tissue (35). In communicating hydrocephalus, the ICP does not increase as significantly as in obstructive hydrocephalus, which may result in a relatively lower CBF in communicating hydrocephalus.

The ΔCBF represents the difference in CBF values between the longer and shorter PLD. A recent study reported that a larger ΔCBF was associated with a longer ATT (16). ATT can directly reflect the state of the arterial circulation and vascular pathologies (36,37). The hypoperfusion area at longer PLD indicates a more severely delayed blood flow (15,38). Regional ATT information can only be obtained through multi-PLD ASL, as single PLD approaches are not able to accurately quantify CBF

Table 2 Subgroup analysis for the association of the degree of ventricular dilatation with ΔCBF in the different groups of hydrocephalus

Brain region	Communicating hydrocephalus				Obstructive hydrocephalus			
	Unadjusted β value	P value	Adjusted β	P value (FDR)	Unadjusted β value	P value	Adjusted β value	P value (FDR)
Anterior external watershed								
R	−0.269 (−0.527, −0.012)	0.041*	−0.101 (−0.353, 0.152)	0.428	0.031 (−0.239, 0.301)	0.817	0.134 (−0.139, 0.406)	0.330
L	−0.144 (−0.409, 0.121)	0.281	0.079 (−0.159, 0.317)	0.507	0.064 (−0.206, 0.333)	0.638	0.156 (−0.118, 0.431)	0.259
Posterior external watershed								
R	0.042 (−0.226, 0.309)	0.757	0.260 (0.021, 0.499)	0.034*	0.104 (−0.165, 0.373)	0.442	0.276 (0.047, 0.505)	0.019*
L	−0.201 (−0.463, 0.061)	0.130	0.012 (−0.218, 0.242)	0.915	−0.121 (−0.389, 0.147)	0.370	0.053 (−0.19, 0.296)	0.664
Internal watershed								
R	0.022 (−0.246, 0.290)	0.870	0.217 (−0.033, 0.467)	0.088	0.024 (−0.246, 0.294)	0.860	0.117 (−0.163, 0.396)	0.407
L	0.107 (−0.16, 0.373)	0.426	0.274 (0.013, 0.536)	0.040*	0.042 (−0.228, 0.312)	0.758	0.096 (−0.187, 0.379)	0.500
Frontal cortex								
R	−0.23 (−0.491, 0.03)	0.082	−0.005 (−0.235, 0.225)	0.966	0.076 (−0.193, 0.346)	0.573	0.231 (−0.015, 0.477)	0.065
L	−0.246 (−0.505, 0.014)	0.063	−0.064 (−0.311, 0.184)	0.607	0.066 (−0.204, 0.335)	0.627	0.189 (−0.079, 0.456)	0.163
Parietal cortex								
R	−0.121 (−0.387, 0.144)	0.364	0.109 (−0.123, 0.34)	0.350	0.078 (−0.191, 0.348)	0.562	0.277 (0.056, 0.498)	0.015*
L	−0.17 (−0.434, 0.094)	0.202	0.084 (−0.128, 0.297)	0.428	−0.196 (−0.461, 0.069)	0.144	−0.013 (−0.248, 0.221)	0.910
Temporal cortex								
R	−0.263 (−0.522, −0.005)	0.046*	−0.1 (−0.349, 0.15)	0.426	−0.104 (−0.373, 0.165)	0.442	0.025 (−0.237, 0.288)	0.847
L	−0.119 (−0.385, 0.147)	0.373	0.062 (−0.194, 0.319)	0.628	−0.072 (−0.341., 0.198)	0.597	0.044 (−0.224, 0.312)	0.743
Occipital cortex								
R	−0.099 (−0.365, 0.168)	0.461	0.109 (−0.136, 0.353)	0.377	−0.018 (−0.288, 0.252)	0.895	0.164 (−0.079, 0.406)	0.181
L	−0.157 (−0.421, 0.107)	0.239	0.048 (−0.188, 0.285)	0.683	−0.08 (−0.349, 0.189)	0.554	0.1 (−0.141, 0.342)	0.408
Cerebellum								
R	−0.208 (−0.47, 0.054)	0.118	0.015 (−0.21, 0.24)	0.894	−0.159 (−0.426, 0.108)	0.237	−0.017 (−0.273, 0.239)	0.895
L	−0.134 (−0.4, 0.131)	0.314	0.034 (−0.228, 0.296)	0.796	−0.05 (−0.32, 0.22)	0.711	0.109 (−0.146, 0.363)	0.396
Thalamus								
R	−0.206 (−0.468, 0.056)	0.120	−0.052 (−0.314, 0.21)	0.691	−0.103 (−0.372, 0.165)	0.444	0.049 (−0.199, 0.297)	0.691
L	−0.195 (−0.458, 0.067)	0.142	0.007 (−0.237, 0.252)	0.951	0.013 (−0.257, 0.283)	0.924	0.131 (−0.129, 0.39)	0.318

Data in parentheses are the 95% CI. β values were adjusted for age, sex, and duration. *, P<0.05. ΔCBF, delta cerebral blood flow; FDR, false discovery rate; R, right; L, left; CI, confidence interval.

in regions affected by this delay. A two-PLD scheme, as proposed by the International Society for Magnetic Resonance in Medicine (ISMRM) Perfusion Study Group (13), can be used as an alternative. Therefore, we believe that the ΔCBF may reflect the ATT and vascular physiology to a certain extent in patients with hydrocephalus. However, this needs to be validated in future studies through actual ATT measurements.

Since a single PLD of 1.5 s can lead to underestimation of the CBF when blood flows slowly, some researchers examined another PLD of 2.5 s to assess the slowly streaming collateral pathway that maintains the cerebrovascular reserve (14,39). Lyu *et al.* used differences based on two PLDs and found that late-arriving antegrade

Table 3 The interaction between age and the different hydrocephalus groups

Brain region	Side	P (FDR-corrected)		R^2	Adjusted R^2
		Age × communicating hydrocephalus	Age × obstructive hydrocephalus		
Anterior external watershed	R	0.004**	0.064	0.247	0.224
	L	0.007**	0.474	0.315	0.293
Posterior external watershed	R	0.039*	0.188	0.348	0.328
	L	0.003**	0.010*	0.352	0.332
Internal watershed	R	0.062	0.304	0.197	0.172
	L	0.121	0.659	0.287	0.265
Frontal cortex	R	0.001**	0.010*	0.350	0.330
	L	0.005**	0.038*	0.349	0.329
Parietal cortex	R	0.034*	0.096	0.315	0.294
	L	0.014*	0.036*	0.336	0.315
Temporal cortex	R	0.013*	0.064	0.277	0.254
	L	0.004**	0.087	0.264	0.241
Occipital cortex	R	0.182	0.270	0.241	0.218
	L	0.049*	0.104	0.253	0.230
Cerebellum	R	0.011*	0.570	0.294	0.273
	L	0.408	0.496	0.219	0.195
Thalamus	R	0.032*	0.124	0.297	0.275
	L	0.009**	0.207	0.292	0.270

The association of age and group (with the healthy group as the reference) and their interaction with ΔCBF in various brain regions. Model construction: ΔCBF ~ age + communicating group + obstructive group+ age × communicating group + age × obstructive group. This table displays the interaction between age and the two grouping variables. *, P<0.05; **, P<0.01. P values were corrected using the FDR method. FDR, false discovery rate; R, right; L, left; ΔCBF, delta cerebral blood flow; ΔCBF, $CBF_{PLD=2.5\,s} - CBF_{PLD=1.5\,s}$.

and retrograde collateral flow were involved in the narrow side of the middle cerebral artery (MCA) (38). We speculate that collateral, compensatory blood flow, or late-arriving slow blood flow also represent a form of CBF regulation. Thus, the ΔCBF may reflect the cerebral regulation of blood flow to some extent. Therefore, patients with hydrocephalus require not only a single PLD to reflect actual perfusion but also a longer PLD to identify regions with delayed blood flow.

Our research indicates that a longer ATT may be required in those with hydrocephalus. Among the two subgroups of hydrocephalus, the ΔCBF of the communicating hydrocephalus group was significantly higher than that of the obstructive hydrocephalus group only in the left internal watershed, indicating that communicating hydrocephalus demonstrates a greater capacity for brain regulation in this brain region as compared to obstructive hydrocephalus. Because the internal watershed is located between the lateral ventricles and the cerebral cortex, it may be susceptible to double compression when there is CSF accumulation in the ventricles and impaired absorption within the sulcus fissure. Under the condition of shear and stretch, the endogenous mediators of vessels activate to regulate blood flow by controlling the vascular smooth muscle tone (40,41).

In obstructive hydrocephalus, CSF production continues despite obstruction, causing increased pressure in the ventricles and brain (42) and resulting in hypoperfusion. The posterior external watershed is the region supplied by the MCA and the terminal branches of the posterior cerebral arteries (PCAs). It is vulnerable to hypoperfusion, ischemia, and vascular changes due to being considered

the cerebral blood supply's "weak point" (43). Miner *et al.*'s study also suggested that the watershed region is highly susceptible to hemodynamic disturbances (44). The parietal cortex is supplied by distal cortical branches of the internal carotid artery (ICA). One study reported that the CBF in the parietal lobe of rats was significantly reduced under stimulation with histamine (45). Both the posterior external watershed and the parietal cortex are susceptible to hemodynamic impairment. Additionally, in obstructive hydrocephalus, ventricles enlargement may compress cortical veins, blocking venous return and causing congestion. This in turn can lead to the expansion of cerebral veins and capillaries and thus increased vascular resistance and elevated ATT (33). Hence, with the dilatation of ventricles, the ΔCBF in the posterior external watershed and parietal cortex increases in obstructive hydrocephalus.

Communicating hydrocephalus occurs due to increased CSF production or decreased CSF absorption (46). The internal watershed is located at the junction of the superficially penetrating branches of the anterior cerebral artery (ACA) and MCA. When the perfusion pressure of the farthest branch of the ICA is low and the supply of collateral branches of the deep perforating lenticulostriate artery is insufficient, the internal watershed is susceptible to hemodynamic damage (25). This is because the ventricular fluid is incompressible while the brain is highly plastic. CSF enters the parenchyma, causing periventricular white-matter edema. This accumulation of interstitial fluid may compress small vessels and hinder the clearance of vasoactive metabolites (47). The production of nitric oxide and amyloid-b protein stagnates in edema, damages vessels, and weakens self-regulation and cerebrovascular reactivity. This can thus potentially explain why the ΔCBF in the internal watershed was associated with ventricular dilatation in those with communicating hydrocephalus.

This study involved certain limitations which should be addressed. First, since data were only collected from hydrocephalus patients with enlarged ventricles, it was not feasible to align the ROI to a standard (Montreal Neurological Institute) space, and instead, the ROI was outlined manually. To ensure measurement reproducibility and accuracy, two neuroradiologists manually outlined the ROI on two consecutive slices and then calculated the average. Second, due to the single-center, retrospective design, data selection bias was inevitable. Future prospective multicenter studies can be conducted to verify the ΔCBF characteristics of hydrocephalus.

In conclusion, we identified hemodynamic alterations in patients with hydrocephalus on 3D pCASL dual PLD, a simple and noninvasive method, and explored the related brain regions representative of the watershed as biomarkers of the degree of ventricular dilation in hydrocephalus. In particular, the difference in CBF between short and long PLD measurements may potentially reflect cerebral self-regulation in the hypoperfusion pathology of hydrocephalus. Our findings provide a new perspective for the hemodynamic study of hydrocephalus and may aid in severity assessment and inform clinical treatment protocols.

Acknowledgments

The authors would like to thank the MR technologists at The Second Affiliated Hospital of Nanchang University for their help in acquiring the images.
Funding: None.

Footnote

Reporting Checklist: The authors have completed the STROBE reporting checklist. Available at https://qims.amegroups.com/article/view/10.21037/qims-24-151/rc

Conflicts of Interest: All authors have completed the ICMJE uniform disclosure form (available at https://qims.amegroups.com/article/view/10.21037/qims-24-151/coif). J.D. is an employee of GE HealthCare. The other authors have no conflicts of interest to declare.

Ethical Statement: The authors are accountable for all aspects of the work in ensuring that questions related to the accuracy or integrity of any part of the work are appropriately investigated and resolved. This study was conducted in accordance with the Declaration of Helsinki (as revised in 2013), approved by the Ethics Committee of The Second Affiliated Hospital of Nanchang University, and registered in the Chinese Clinical Trials Register (registration No. ChiCTR2300070646; http://www.chictr.org.cn). All participants were exempt from informed consent due to the study's retrospective nature.

References

1. Agarwal A, Bathla G, Kanekar S. Imaging of Communicating Hydrocephalus. Semin Ultrasound CT MR 2016;37:100-8.
2. Kahle KT, Kulkarni AV, Limbrick DD Jr, Warf BC. Hydrocephalus in children. Lancet 2016;387:788-99.
3. McAllister JP 2nd. Pathophysiology of congenital and neonatal hydrocephalus. Semin Fetal Neonatal Med 2012;17:285-94.
4. Koleva M, De Jesus O. Hydrocephalus. StatPearls. Treasure Island (FL) ineligible companies. Disclosure: Orlando De Jesus declares no relevant financial relationships with ineligible companies. StatPearls Publishing LLC., 2024.
5. Wozniak M, McLone DG, Raimondi AJ. Micro- and macrovascular changes as the direct cause of parenchymal destruction in congenital murine hydrocephalus. J Neurosurg 1975;43:535-45.
6. Yeom KW, Lober RM, Alexander A, Cheshier SH, Edwards MS. Hydrocephalus decreases arterial spin-labeled cerebral perfusion. AJNR Am J Neuroradiol 2014;35:1433-9.
7. Takahashi R, Ishii K, Tokuda T, Nakajima M, Okada T; SINPHONI-2 Investigators. Regional dissociation between the cerebral blood flow and gray matter density alterations in idiopathic normal pressure hydrocephalous: results from SINPHONI-2 study. Neuroradiology 2019;61:37-42.
8. van Asch CJ, van der Schaaf IC, Rinkel GJ. Acute hydrocephalus and cerebral perfusion after aneurysmal subarachnoid hemorrhage. AJNR Am J Neuroradiol 2010;31:67-70.
9. Kang K, Jeong SY, Park KS, Hahm MH, Kim J, Lee HW, Kim CH, Yun E, Han J, Yoon U, Lee SW. Distinct cerebral cortical perfusion patterns in idiopathic normal-pressure hydrocephalus. Hum Brain Mapp 2023;44:269-79.
10. Czosnyka ZH, Czosnyka M, Whitfield PC, Donovan T, Pickard JD. Cerebral autoregulation among patients with symptoms of hydrocephalus. Neurosurgery 2002;50:526-32; discussion 532-3.
11. Wang H, Han X, Li M, Yang ZH, Liu WH, Wang ZC. Long-term hemodialysis may affect enlarged perivascular spaces in maintenance hemodialysis patients: evidence from a pilot MRI study. Quant Imaging Med Surg 2022;12:341-53.
12. Meixner CR, Nagel AM, Höger SA, Gast LV, Wiesmueller M, Uder M, May MS, Hotfiel T, Heiss R. Muscle perfusion and the effect of compression garments in delayed-onset muscle soreness assessed with arterial spin labeling magnetic resonance imaging. Quant Imaging Med Surg 2022;12:4462-73.
13. Lindner T, Bolar DS, Achten E, Barkhof F, Bastos-Leite AJ, Detre JA, et al. Current state and guidance on arterial spin labeling perfusion MRI in clinical neuroimaging. Magn Reson Med 2023;89:2024-47.
14. Haga S, Morioka T, Shimogawa T, Akiyama T, Murao K, Kanazawa Y, Sayama T, Arakawa S. Arterial Spin Labeling Perfusion Magnetic Resonance Image with Dual Postlabeling Delay: A Correlative Study with Acetazolamide Loading (123)I-Iodoamphetamine Single-Photon Emission Computed Tomography. J Stroke Cerebrovasc Dis 2016;25:1-6.
15. Lou X, Ma X, Liebeskind DS, Ma N, Tian C, Lyu J, Long X, Ma L, Wang DJ. Collateral perfusion using arterial spin labeling in symptomatic versus asymptomatic middle cerebral artery stenosis. J Cereb Blood Flow Metab 2019;39:108-17.
16. Zhang R, Huang P, Wang S, Jiaerken Y, Hong H, Zhang Y, Yu X, Lou M, Zhang M. Decreased Cerebral Blood Flow and Delayed Arterial Transit Are Independently Associated With White Matter Hyperintensity. Front Aging Neurosci 2022;14:762745.
17. Itagaki H, Kokubo Y, Kawanami K, Sato S, Yamada Y, Sato S, Sonoda Y. Arterial spin labeling magnetic resonance imaging at short post-labeling delay reflects cerebral perfusion pressure verified by oxygen-15-positron emission tomography in cerebrovascular steno-occlusive disease. Acta Radiol 2021;62:225-33.
18. Long J, Lin H, Cao G, Wang MZ, Huang XJ, Xia J, Sun Z. Relationship between intracranial pressure and phase-contrast cine MRI-derived measures of cerebrospinal fluid parameters in communicating hydrocephalus. Quant Imaging Med Surg 2019;9:1413-20.
19. Alsop DC, Detre JA. Reduced transit-time sensitivity in noninvasive magnetic resonance imaging of human cerebral blood flow. J Cereb Blood Flow Metab 1996;16:1236-49.
20. Wu B, Lou X, Wu X, Ma L. Intra- and interscanner reliability and reproducibility of 3D whole-brain pseudo-continuous arterial spin-labeling MR perfusion at 3T. J

Magn Reson Imaging 2014;39:402-9.
21. Wang X, Dou W, Dong D, Wang X, Chen X, Chen K, Mao H, Guo Y, Zhang C. Can 3D Pseudo-Continuous Territorial Arterial Spin Labeling Effectively Diagnose Patients With Recanalization of Unilateral Middle Cerebral Artery Stenosis? J Magn Reson Imaging 2021;54:175-83.
22. Lu H, Clingman C, Golay X, van Zijl PC. Determining the longitudinal relaxation time (T1) of blood at 3.0 Tesla. Magn Reson Med 2004;52:679-82.
23. Alsop DC, Detre JA, Golay X, Günther M, Hendrikse J, Hernandez-Garcia L, Lu H, MacIntosh BJ, Parkes LM, Smits M, van Osch MJ, Wang DJ, Wong EC, Zaharchuk G. Recommended implementation of arterial spin-labeled perfusion MRI for clinical applications: A consensus of the ISMRM perfusion study group and the European consortium for ASL in dementia. Magn Reson Med 2015;73:102-16.
24. Hou Y, Guo K, Fan X, Shang K, Wang J, Wang Z, Shan Y, Zhao G, Lu J. Crossed cerebellar diaschisis: risk factors and prognostic value in focal cortical dysplasia by (18) F-FDG PET/CT. Ann Nucl Med 2021;35:719-27.
25. Li Y, Li M, Zhang X, Yang S, Fan H, Qin W, Yang L, Yuan J, Hu W. Clinical features and the degree of cerebrovascular stenosis in different types and subtypes of cerebral watershed infarction. BMC Neurol 2017;17:166.
26. Sorgun MH, Rzayev S, Yilmaz V, Isıkay CT. Etiologic Subtypes of Watershed Infarcts. J Stroke Cerebrovasc Dis 2015;24:2478-83.
27. Brix MK, Westman E, Simmons A, Ringstad GA, Eide PK, Wagner-Larsen K, Page CM, Vitelli V, Beyer MK. The Evans' Index revisited: New cut-off levels for use in radiological assessment of ventricular enlargement in the elderly. Eur J Radiol 2017;95:28-32.
28. Takaya M, Kazui H, Tokunaga H, Yoshida T, Kito Y, Wada T, Nomura K, Shimosegawa E, Hatazawa J, Takeda M. Global cerebral hypoperfusion in preclinical stage of idiopathic normal pressure hydrocephalus. J Neurol Sci 2010;298:35-41.
29. Lee D, Kim ES, Lee Y, Lee SM, Yoon DY, Ju YS, Chang IB. Changes in computed tomography perfusion parameters and maximum contrast enhancement in patients having hydrocephalus with a ventriculoperitoneal shunt: a pilot study. Acta Radiol 2022;63:1398-405.
30. Stivaros SM, Sinclair D, Bromiley PA, Kim J, Thorne J, Jackson A. Endoscopic third ventriculostomy: predicting outcome with phase-contrast MR imaging. Radiology 2009;252:825-32.
31. Chang CC, Asada H, Mimura T, Suzuki S. A prospective study of cerebral blood flow and cerebrovascular reactivity to acetazolamide in 162 patients with idiopathic normal-pressure hydrocephalus. J Neurosurg 2009;111:610-7.
32. Greitz D, Greitz T, Hindmarsh T. A new view on the CSF-circulation with the potential for pharmacological treatment of childhood hydrocephalus. Acta Paediatr 1997;86:125-32.
33. Greitz D. Radiological assessment of hydrocephalus: new theories and implications for therapy. Neurosurg Rev 2004;27:145-65; discussion 166-7.
34. Green LM, Wallis T, Schuhmann MU, Jaeger M. Intracranial pressure waveform characteristics in idiopathic normal pressure hydrocephalus and late-onset idiopathic aqueductal stenosis. Fluids Barriers CNS 2021;18:25.
35. Donnelly J, Czosnyka M, Harland S, Varsos GV, Cardim D, Robba C, Liu X, Ainslie PN, Smielewski P. Cerebral haemodynamics during experimental intracranial hypertension. J Cereb Blood Flow Metab 2017;37:694-705.
36. Zhao MY, Armindo RD, Gauden AJ, Yim B, Tong E, Moseley M, Steinberg GK, Zaharchuk G. Revascularization improves vascular hemodynamics - a study assessing cerebrovascular reserve and transit time in Moyamoya patients using MRI. J Cereb Blood Flow Metab 2023;43:138-51.
37. Kim DW, Shim WH, Yoon SK, Oh JY, Kim JK, Jung H, Matsuda T, Kim D. Measurement of arterial transit time and renal blood flow using pseudocontinuous ASL MRI with multiple post-labeling delays: Feasibility, reproducibility, and variation. J Magn Reson Imaging 2017;46:813-9.
38. Lyu J, Ma N, Liebeskind DS, Wang DJ, Ma L, Xu Y, Wang T, Miao Z, Lou X. Arterial Spin Labeling Magnetic Resonance Imaging Estimation of Antegrade and Collateral Flow in Unilateral Middle Cerebral Artery Stenosis. Stroke 2016;47:428-33.
39. Shimogawa T, Morioka T, Akiyama T, Haga S, Arakawa S, Sayama T. Sequential changes of arterial spin-labeling perfusion MR images with dual postlabeling delay following reconstructive surgery for giant internal carotid artery aneurysm. Surg Neurol Int 2017;8:222.
40. Ainslie PN, Ogoh S. Regulation of cerebral blood flow in mammals during chronic hypoxia: a matter of balance. Exp Physiol 2010;95:251-62.
41. Rebel A, Ulatowski JA, Kwansa H, Bucci E, Koehler RC. Cerebrovascular response to decreased hematocrit: effect of cell-free hemoglobin, plasma viscosity, and CO2. Am J

Physiol Heart Circ Physiol 2003;285:H1600-8.
42. Maller VV, Gray RI. Noncommunicating Hydrocephalus. Semin Ultrasound CT MR 2016;37:109-19.
43. Kapasi A, Yu L, Petyuk V, Arfanakis K, Bennett DA, Schneider JA. Association of small vessel disease with tau pathology. Acta Neuropathol 2022;143:349-62.
44. Miners JS, Palmer JC, Love S. Pathophysiology of Hypoperfusion of the Precuneus in Early Alzheimer's Disease. Brain Pathol 2016;26:533-41.
45. Yang PB, Chen XL, Zhao JJ, Zhang JS, Zhang JF, Tian YM, Liu Y. Effect of histamine on regional cerebral blood flow of the parietal lobe in rats. Lasers Med Sci 2010;25:711-7.
46. Kondziella D, Lüdemann W, Brinker T, Sletvold O, Sonnewald U. Alterations in brain metabolism, CNS morphology and CSF dynamics in adult rats with kaolin-induced hydrocephalus. Brain Res 2002;927:35-41.
47. Virhammar J, Laurell K, Ahlgren A, Larsson EM. Arterial Spin-Labeling Perfusion MR Imaging Demonstrates Regional CBF Decrease in Idiopathic Normal Pressure Hydrocephalus. AJNR Am J Neuroradiol 2017;38:2081-8.

Cite this article as: Xiao Y, Chen S, Zhang Z, Huang J, Gui Y, Luo D, Deng X, Dai J, Xiao X. Three-dimensional pseudocontinuous arterial spin labeling with dual postlabeling delay for reflecting cerebral blood flow regulation in patients with hydrocephalus: a retrospective cross-sectional study. Quant Imaging Med Surg 2024;14(8):5861-5876. doi: 10.21037/qims-24-151

